

行政院國家科學委員會專題研究計畫成果報告

超快光學與超快光電子學之研究(總計劃)

Ultrafast Optics and opto-electronics

計畫編號：NSC 87-2215-E-009-004

執行期限：86年08月01日至87年07月31日

主持人：潘犀靈 國立交通大學光電工程研究所

一、中文摘要

本年度計畫成果摘要包括下列幾項：

1. 同步的時域偵測與雷射時序紊亂度的抑制

我們在鎖相迴路中利用皮秒電脈衝驅動光電諧波混頻器以達到同步偵測，並可將雷射的相位雜訊降低兩個數量級

2. 觀察以三層扭曲量子阱飽和布拉格反射體(SSBR)產生飛秒脈衝的特性

我們觀察 SSBR 的超低飽和強度並在忽略克爾透鏡效應的情形下觀察有 SSBR 下鈦藍寶石雷射的啟動動力學

3. 觀察扭曲式量子阱飽和布拉格反射體(SSBR)的強大非線性現象與超快載子動力學

我們報導SSBR的暫態反射率可到4%，並在多波長的情況下展現載子動態力學的特性

4. 在漸寬增益區半導體雷射放大器的次皮秒脈衝光放大

我們報導在漸寬增益區半導體雷射放大器的非秒脈衝放大，最大增益可到14倍而最小的脈衝寬度可到267fs。更進一步我們展現在驅動電流接近閾值電流時的放大輸出可到68%，而在雷射驅動電流接近1.65倍的閾值電流時便驟降到到10%。

5. 利用液晶空間光調制器產生數位可調半導體雷射

具有窄線寬，數位可調波長之雷射輸出已經獲得；此雷射採用一種摺疊望遠鏡式的光柵，外腔為一液晶空間光反射器。

6. 本計劃中我們運用光纖光柵所構成之反射式 Fabry-Perot 濾波器來穩定主動諧波鎖模摻鉍光纖雷射，我們可以得到穩定之脈衝序列輸出，此脈衝之寬度為 91 ps、重複頻率為 800 MHz、平均輸出功率約 3mW，旁模抑制比(side-mode suppression ratio)可達 40 dB 以上，平均輸出功率之混亂度在 0.5%以內，已經相當接近實用階段。

關鍵詞：雷射時序紊亂度、扭曲式量子阱飽和布拉格反射體(SSBR)、啟動動力學、超快載子動力學、漸寬增益區半導體雷射放大器、液晶空間光調制器、光纖光柵、鎖模雷射、光纖雷射、摻鉍光纖

Abstract

The abstract of this project report contain those items as following:

1. Simultaneous time-domain detection and suppression of laser timing jitter

We employ an optoelectronic harmonic mixer, biased by picosecond electrical pulses, in a phase-locked loop for simultaneous detection and suppression of laser phase noise by two orders of magnitudes.

2. Characterization of a triple strained-quantum-well saturable Bragg reflector (SSBR) for the generation of femtosecond pulses

We characterized the SSBR with ultra-low saturation fluence and the build-up dynamics of a Ti: sapphire laser with the SSBR and

negligible Kerr-lens strength.

3. Giant Optical Nonlinearity and Ultrafast Carrier Dynamics of a Strained Quantum Well Saturable Bragg Reflector (SSBR)

We report normalized nonlinear reflectivity as large as 4% for a SSBR. Experiments were performed at multiple wavelengths to elucidate carrier dynamics.

4. Subpicosecond Pulse Amplification

In a Tapered-waveguide Laser Diode Amplifier

Femtosecond pulses amplification in a tapered-waveguide laser diode amplifier with a maximum gain of 14 and minimum output pulse width of 267 fs is reported. Further, we show that the percentage of the amplified output that is ultrafast is about 68% at $I \sim I_{th}$ and rapidly decreased to 10% for $I \sim 1.65 I_{th}$.

5. Digitally Tunable Laser Diode With a Liquid Crystal Spatial Light Reflector

Narrow-linewidth, digitally wavelength-tunable output is obtained by a laser diode with an external folded telescopic grating loaded external cavity incorporating a liquid spatial light reflector (LC-SLR).

6. In this project, we use a reflective Fabry-Perot filter composed by two fiber gratings to stabilize an active harmonic modelocked Erbium-doped fiber laser. Stable output pulses are obtained with a 91 ps pulse duration, 800 MHz repetition rate, 3 mW output average power, 40 dB side-mode suppression ratio, and less than 0.5% average power fluctuations. The experimental results agree reasonably well with the theoretical predictions from the Kuizenga-Siegman's theory of actively modelocked lasers.

Keywords: laser timing jitter, Strained

Quantum Well Saturable Bragg Reflector (SSBR), build-up dynamics, Ultrafast Carrier Dynamics, Tapered-waveguide Laser Diode Amplifier, Liquid Crystal Spatial Light Reflector(LC-SLM), Fiber Grating, Modelocked Laser, Fiber Laser, Erbium Doped Fiber.

二、内容

1. Simultaneous time-domain detection and suppression of laser timing jitter

緣由與目的

Phase noise or timing jitter is an important attribute of mode-locked lasers. Active laser timing stabilization or synchronization schemes are often required in applications [1]. In this work, we demonstrate a new phase stabilization technique that allows us to phase-lock up to the 33rd laser harmonic component. Simultaneous detection of phase noise for determination of laser timing jitter is also achieved in lieu of the use of commercial vector signal analyzers as in the recent work of Tsuchida [2]

結果與討論

Our experimental setup is shown in Fig. 1. The laser was a femtosecond passively mode-locked Ti:sapphire laser with a strained saturable Bragg Reflector (SSBR) [3]. The key component in our phase detection and suppression scheme is a GaAs:Cr photoconductive switch that acts as the optoelectronic harmonic mixer (OEHM). It is used for intermixing the harmonics of the laser pulse train at f_0 and harmonics of the RF signal from a comb generator ($f = 1000$ MHz) to generate an intermediate frequency (IF)

signal at 150 kHz ($f_{IF} = Nf - Mf_0$). For the phase noise detection part of this scheme, the IF signal is fed to a digital phase comparator where it is compared in phase with a synchronous reference signal ($f_R = 10$ MHz) through a frequency divider. The error signal generated from the digital phase comparator was then fed to a 12-bit A-D card. After signal processing using FFT algorithms, the phase noise spectrum could be obtained. For comparison, conventional power spectral analysis is also performed.

The timing jitter of the laser without active phase control was determined by conventional power spectral measurements to be above 7.5 ps and up to several tens of picoseconds by deliberately adjusting the intracavity bandwidth. The single-sideband (SSB) phase-noise spectrum of the stabilized laser is shown in Fig. 2. For this case, the 3rd-harmonics of the RF signal was intermixed with the 33th-harmonics of the laser pulse train. The corresponding RMS timing jitter is 662fs (100-500Hz) and 661fs (0.5-5kHz), respectively. The error signal taken from the digital phase comparator sampled at 10 kHz in 0.5 sec is shown in the inset of Fig.2, which indicates a time-averaged timing fluctuation of about 0.35ps. After performing FFT on the phase-noise data, we determined that the RMS timing jitter of the stabilized laser is 254fs (100-500Hz) and 236fs (0.5-5kHz), respectively. The discrepancy is due to (1) the frequency domain approach is valid for active mode-locked laser for which the central frequency of laser pulse train is quasi-stationary; and (2) amplitude noise that can not be subtracted out completely in the power spectral analysis. In Fig. 3, we show frequency- and time-domain results of SSB phase noise spectral density for the stabilized laser by locking the

11th, 22nd, and 33rd laser harmonics. The timing jitter decreased with the use of higher harmonics as expected. On the other hand, the time-domain jitter data are consistently two times smaller than those from the conventional spectral analysis.

In summary, we show a new technique which can be used to stabilize the laser at high harmonics by extending the fundamental RF signal frequency via a comb generator. The same scheme also provides the time domain phase noise detection capability. This work was supported in part by the National Science Council of the Republic of China.

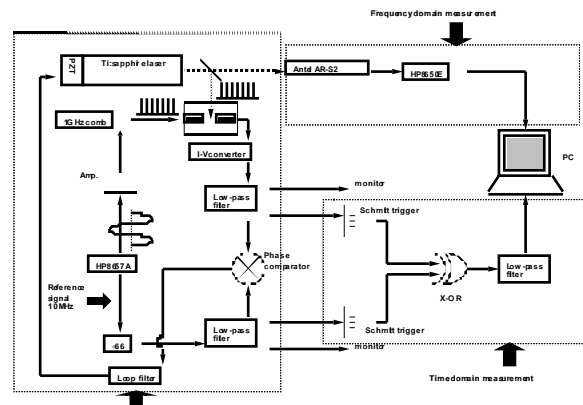


Fig.1 Schematic diagram of the high harmonic OEPLL for active timing stabilization and time domain phase noise measurement

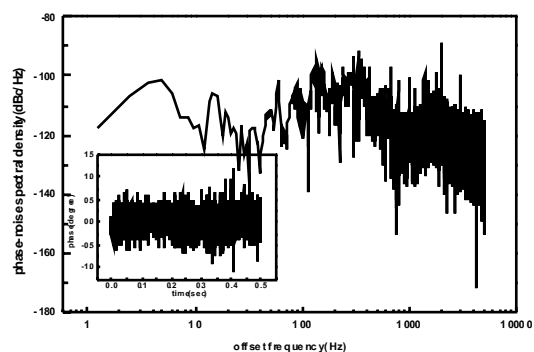


Fig.2 Single-sideband phase-noise spectral density for the stabilized laser and harmonic of RF signal by conventional frequency domain approach.

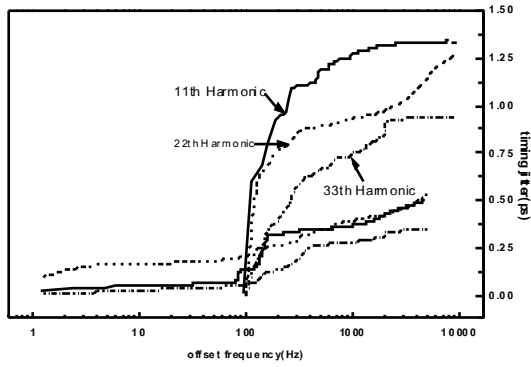


Fig.3 Single-sideband phase-noise spectral density for the stabilized laser by time domain approach.

2. Characterization of a triple strained-quantum-well saturable Bragg reflector (SSBR) for the generation of femtosecond pulses

緣由與目的

Lately, there have been substantial interests in passively mode-locked solid state lasers with semiconductor saturable absorber mirror (SESAM) [4,5]. Pulses as short as 6.5 fs were generated. In this work, the saturation fluence of a new type of SESAM, the triple strained-quantum-well Bragg reflector (SSBR) [6] was determined by ultrafast nonlinear reflectivity measurements. The ultra-low saturation fluence are consistent with wavelength-dependent buildup dynamics of the laser with the SSBR and negligible Kerr-lens-mode-locking (KLM) strength. Such lasers are capable of sustaining stable sub-100fs pulses.

結果與討論

The laser configuration with a triple strained-quantum-well saturable Bragg reflector (SSBR) and weak KLM has been described previously [6]. The structure, reflection and continuous wave photoluminescence (PL) spectra are shown in Fig. 1, 2. The output power and pulse width

of the Ti : sapphire/SSBR lasers pumped by an argon laser at 5W were 230 mW and 90 fs respectively. Using pump-probe techniques, we have determined the normalized nonlinear reflectivity $\Delta R/R$ as a function of average power (P_{inc}) incident on the SSBR at several wavelengths in the tuning range of mode-locked laser with this SSBR device (see Fig. 3). From Fig. 3, We find that the saturation optical fluence E_{sat} were all about $12\mu J/cm^2$ ($P_{inc} \sim 40mW$). This is explained by noting that they are associated with the same exciton absorption resonance. On the other hand, the linear absorption strength decreased as the wavelength was shifted away from the peak absorption wavelength ($\lambda = 755$ nm). This trend was also observed in PL measurements.

The transient second harmonic signal for this laser during the buildup are shown in Fig. 4. The wavelengths of the laser was set at $\lambda = 775nm, 786nm,$ and $795nm$ for the buildup experiment. Figure 5 showed the corresponding theoretical buildup trace obtained using the master equation approach with KLM neglected. In separate experiments, we have determined that the unsaturated loss q_0 , the fast decay time and the slow decay time of the SSBR are $0.6 \sim 3 \times 10^{-3}$, 280 fs and 40 ps respectively (The beam spot size on SSBR $\approx 100\mu m$). The theoretical and experimental results are in excellent agreements. The CW stage and total buildup time were 60 us and 100 us at $\lambda = 775nm$. At $\lambda = 786nm$, these values lengthened to $\sim 65us$ and $150us$. The relatively drastic change of in these time scales can be explained by the decrease of rapid recovery of saturation effect. The nonlinear reflectivity traces at the three wavelengths shown in Fig. 6 could identify this. For $\lambda = 795nm$, the corresponding time scales were $\sim 100us$ and $210us$. This can be

explained by the weaker linear absorption strength of the SSBR at the longer wavelength. Since the KLM mechanism was neglected in our simulation, our results indicate that the laser with SSBR could generate stable sub-100 fs pulse without the aid of the KLM mechanism.

In conclusion, nonlinear reflectivity measurements were performed to determine the saturation fluence of triple strained-quantum-well SBR with ultralow saturation fluence of $12 \mu\text{J}/\text{cm}^2$ by studying time-resolved nonlinear reflectivity and pulse-forming dynamics. Studying of the buildup dynamics demonstrated that mode-locking force of SSBR could self-start and stabilize the sub-100 fs pulse forming.

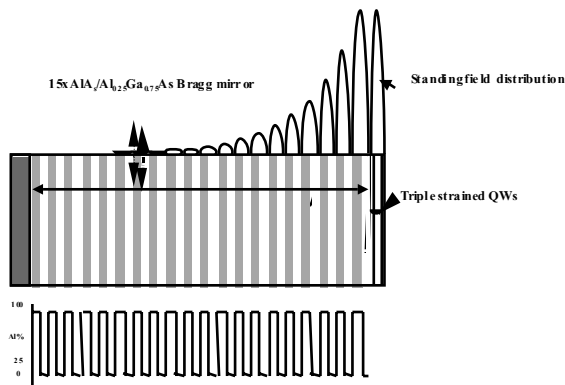


Fig 1. Structure of the strained-layer saturable Bragg reflector (SSBR) with a distributed Bragg reflect (DBR) and an additional $\lambda/2$ layer of $\text{Al}_{0.25}\text{Ga}_{0.75}\text{As}$; three quantum wells with different absorption peak were inserted in this layer.

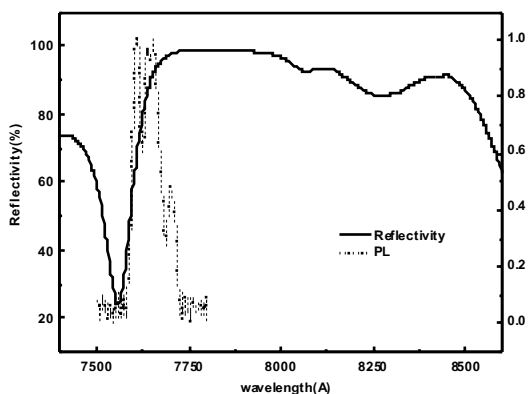


Fig 2. The reflectivity and the CW photoluminescence (PL) spectra of the SSBR.

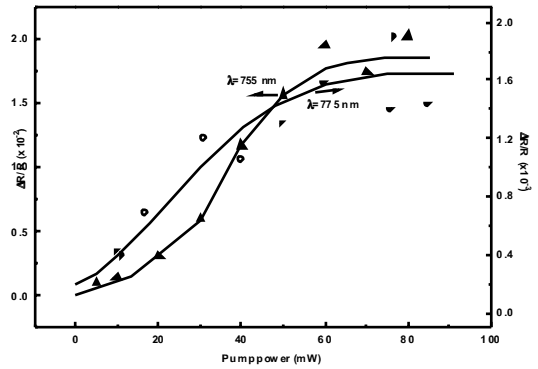


Fig 3. Normalized nonlinear reflectivity of the SSBR at $\lambda = 755 \text{ nm}$ and 775 nm are plotted as a function of incident average power.

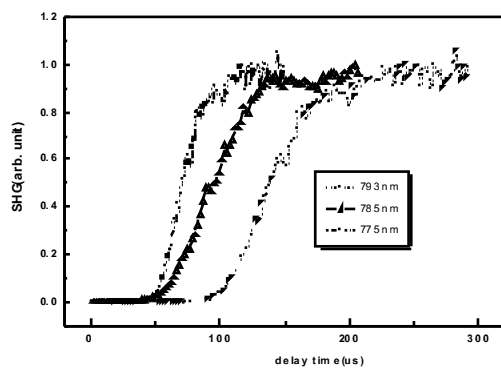


Fig 4. The experimental transient second harmonic signal for three

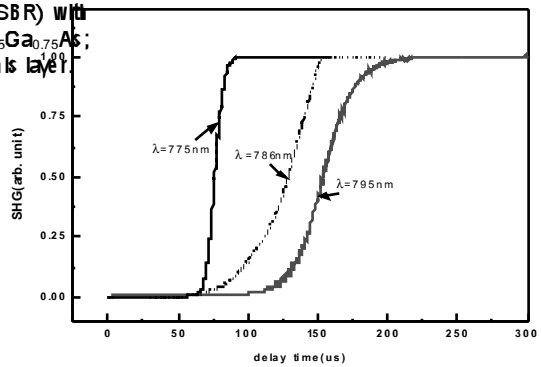


Fig 5. The theoretical transient second harmonic signal for three

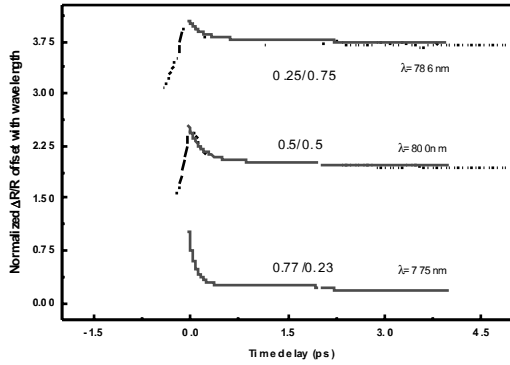


Fig.6 The nonlinear reflectivity trace and fitting curve of three wavelength. The fast/slow ratio of fitting curve are also shown.

3. Giant Optical Nonlinearity and Ultrafast Carrier Dynamics of a Strained Quantum Well Saturable Bragg Reflector (SSBR)

緣由與目的

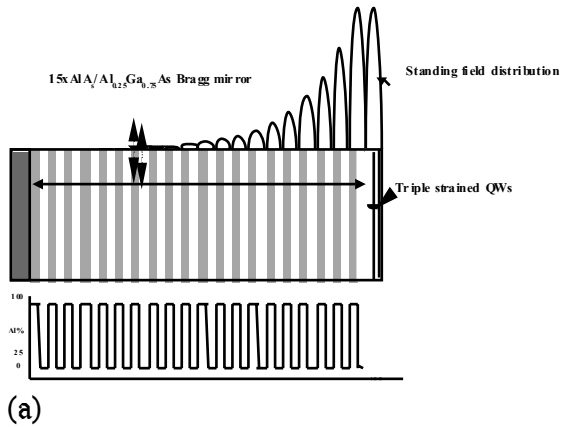
Recently, semiconductor saturable Bragg reflectors (SBR's) have been successfully developed for passive mode-locking of solid state lasers [7~9]. In particular, we have developed a triple strained quantum well saturable Bragg reflector (SSBR) with saturation fluence as low as $12 \mu\text{J}/\text{cm}^2$ [10]. This suggests potential applications of this device for applications such as all-optical switching and modulation. In this work, we report a new type of SBR using triple strained-layer quantum wells as the absorbing layer which named strained saturated bragg reflector(SSBR). Because of its low saturation energy and large tuning range, we want to understand the carrier dynamics with detailed wavelength. The time-resolved differentiation reflection ($\Delta R/R$) in this SSBR with detailed variant pumping energies have been observed. The influence of carrier scattering and process of recombination on the temporal and spectral $\Delta R/R$ dynamics have been investigated.

結果與討論

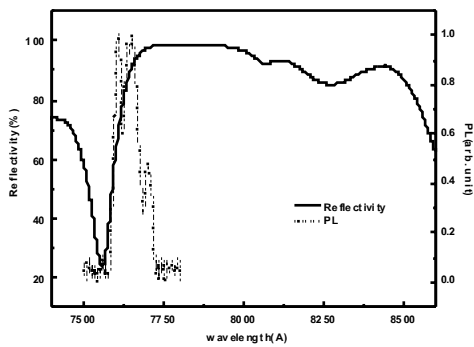
The structure, reflectivity and photoluminescence spectra of the SSBR are shown in Fig. 1. Femtosecond pump/probe experiments were performed. The normalized time-resolved reflectivity, $\Delta R/R$, of the SSBR

sample as a function of the pumping wavelength are shown in Fig. 2. The wavelength-dependent peak values of $\Delta R/R$ are plotted in Fig. 3. When the sample was excited at a photon energy above the band gap ($\lambda < 757.5\text{nm}$), $\Delta R/R$ is positive and with a peak value of ($\sim 4\%$) at 755nm . It must be very large compared with other bulk material, like GaAs. The large optical nonlinearity can be attributed in part to band filling and reduced absorption. Further, the optical excitation of carriers induced charges screening the internal piezoelectric field. This leads to absorption bleaching and can result in very large optical nonlinearities.[11] There have a large peak magnitude of the transient $\Delta R/R$ in 755nm and negative sign from 760nm . This anomalous dispersion trend had been demonstrated in other papers[12] From 755nm to 760nm , the ratio of the peak negative value to the positive value of $\Delta R/R$ increased and then decreased from 760nm to 775nm . A sign reversal for $\Delta R/R$ with peak negative magnitude of -0.6% was observed at 760nm . This can be explained by using the free carrier absorption model. By analyzing the transient $\Delta R/R$ signal, we also determined that the fast and slow carrier lifetimes of the SSBR. The wavelength dependence are shown in Fig. 4(a) and (b). While the wavelength dependence for the fast component of the carrier lifetime is not apparent, the slower component decreased by about an order of magnitude from 250ps at 750nm to 20ps at 775nm .

In summary, normalized nonlinear reflectivity as large as, 4% at 755nm was observed and attributed to band filling, screening effect and surface field enhancement effects. Sign reversal of the transient $\Delta R/R$ signal from 760nm to 775nm are explained by the free carrier absorption effect. The wavelength-dependence of the fast and slow components of the carrier lifetime is significant for the performance of the SSBR as an effective saturable absorber for stable mode-locking.



(a)



(b)

Fig.1 (a) Structure of the strained-layer saturable Bragg reflector (SSBR) with a distributed Bragg reflect (DBR) and an additional $\lambda/2$ layer of $\text{Al}_{0.25}\text{Ga}_{0.75}\text{As}$; three quantum well with different absorption peak were inserted in this layer.

(b) The reflectivity and the CW photo-luminescence (PL) spectra of the SSBR.

Fig.2 Wavelength-dependent time-resolved reflectivity of SSBR

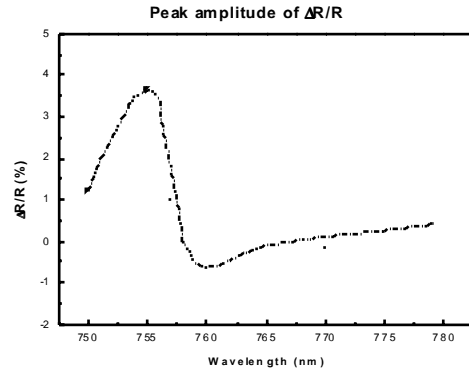
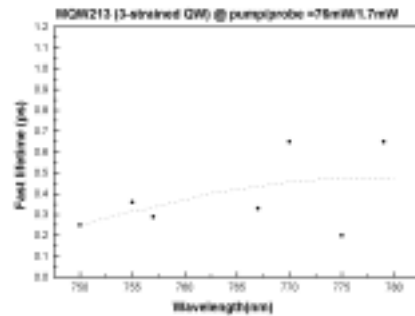
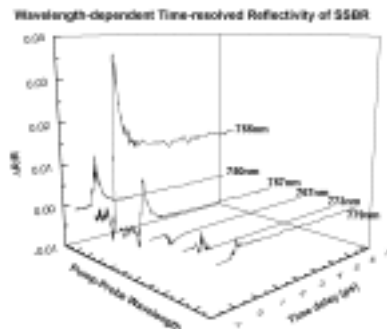
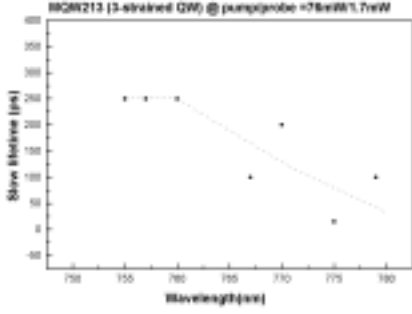


Fig. 3 The peak amplitude of $\Delta R/R$ at different pumping wavelength



(a)





(b)

Fig. 4 The dependence of (a) fast and (b) slow carrier lifetime with pumping wavelength

4. Subpicosecond Pulse Amplification In a Tapered-waveguide Laser Diode Amplifier

緣由與目的

Ultrashort pulse amplification in laser diode amplifiers (LDA's) has attracted considerable attention because of its potential applications in optical communication and signal processing. With the advent of LDA's with tapered-waveguide, several groups have investigated both experimentally and theoretically the prospect of generating high-power picosecond pulses using such devices [13-16]. In this paper, we report the first subpicosecond pulse amplification experiment in LDA's with tapered-waveguide (TW-LDA).

結果與討論

We perform our experiments with a home-made passively mode-locked Ti:sapphire/SBR laser. Transform-limited 150 fs pulses ($\lambda = 812$ nm) at 82 MHz were injected into a one-side AR-coated tapered-waveguide diode chip found in a commercial

tunable diode laser, SDL-8630. The amplified pulses were analyzed with an intensity autocorrelator and optical spectrum analyzer.

Figure 1 depict autocorrelation traces of the transmitted pulses at the output of the TW-LDA as a function of the dc bias current ($0.82I_{th} \leq I \leq 1.64 I_{th}$, $I_{th} = 450$ mA). The pulse shape is Gaussian while the FWHM gradually increases from 260 fs to 440 fs at $I = 1.6$ A. For $I \leq I_{th}$, the output bandwidth is nearly transform-limited with a spectral bandwidth of 4 – 5 nm. Near threshold, this rapidly decreased to 2.2 nm and approaches 1.8 nm at $I \sim I \leq 1.64 I_{th}$. Significant rise of the baseline of the autocorrelation traces for $I \geq I_{th}$ is also evident in Fig. 1. The output then corresponds to perfectly phase-locked components with a broad tail consisting of partially phase-locked and randomly-phased modes. In Fig. 2, we have plotted the inverse contrast ratio, R^{-1} , of the LDA-TW output correlation traces as a function of I/I_{th} . We define R as the peak-to-shoulder value of the autocorrelation traces. Thus $R^{-1} = 0$ for perfectly phase-locked pulse and $R^{-1} = 0.5$ for randomly phase modes. Also plotted in Fig. 2 is the fractional energy, β , which is defined as $\beta = \frac{E_p}{E_{total}}$, where E_p is the energy of the pulse and E_{total} is the energy of pulse with background. It can be calculated from the SHG conversion efficiency as we described previously. [17] Below I_{th} , $R^{-1} \sim 0$ while β is nearly 100%. These two parameters changed drastically near I_{th} , e.g. $\beta \sim 68\%$ or 68% of the pulse energy is within the femtosecond phase-locked pulse. For $I \sim 1.6 I_{th}$, β reduced to 10% while $R^{-1} \sim 0.4$. That is, most of the pulse energy is within the partially phase-locked or randomly phase-locked modes. In Fig. 3, we have plotted gain of the LDA-TW as a function of

bias current. The maximum observed gain at I/I_{th} was nearly 14dB.

In summary, we report first experimental results of subpicosecond pulse amplification in tapered-waveguide laser diode amplifiers. We are also able to determine for the first time fraction of the amplified output that is ultrafast.

Acknowledgements: This work was partially supported by the National Science Council of the R.O.C. under various grants.

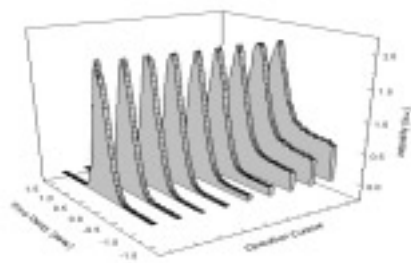


Fig. 1 Autocorrelation traces of the subpicosecond amplified pulses as a function of bias current.

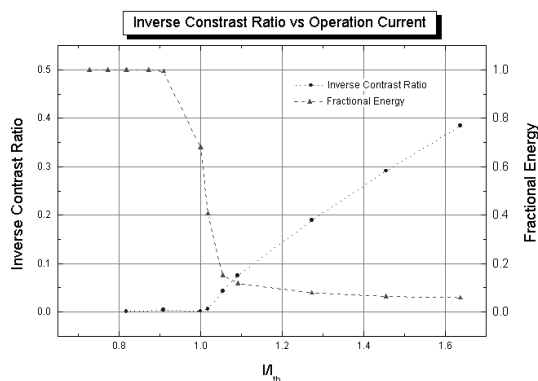


Fig. 2 Inverse contrast ratio and fractional energy of the subpicosecond amplified pulses as a function of bias current

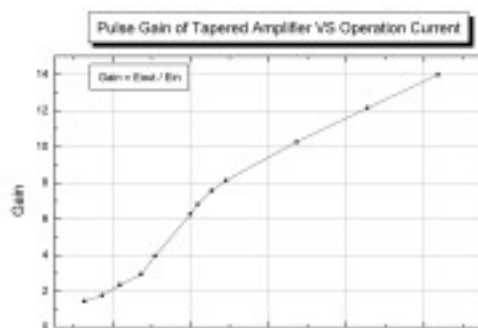


Fig. 3 Pulse gain of the tapered amplifier as a function of bias current.

5. Digitally Tunable Laser Diode With a Liquid Crystal Spatial Light Reflector

緣由與目的

Owing to their applications in coherent optical communication, high-resolution spectroscopy and optical metrology, tunable external cavity semiconductor lasers have been extensively studied in the past decade. Typical tuning methods employ bulk and fiber-type Littrow and grazing-incidence gratings, Fabry-Perot Eaton or interference filter, as well as electro-optic or acousto-optic tunable filter [18]. In this work, we report a novel digitally wavelength-tunable laser diode by using a folded telescopic grazing-incidence grating-loaded external cavity [19] incorporating a liquid crystal spatial light reflector.

結果與討論

A schematic of the laser is shown in Fig. 1. A low-power red laser diode (LD, $\lambda = 650$ nm) from a commercial laser pointer was used without modification. Output of the LD was collimated and incident on the grating (1800 lines/mm) at an angle of 79° . The primary laser output is the zeroth-order reflection of the grating ($\sim 60\%$ of the incident light from the diode chip). The first-order-diffracted light was collected by a lens and focused on the LC-SLR. That is, a reflection-mode

spatial light modulator as shown in Fig. 2. It is based on the design of a normally off twisted nematic liquid crystal (NLC) cell. A 6- μm -thick NLC (E7 manufactured by Merck) layer was sandwiched between a glass cell with indium-tin-oxide (ITO) electrodes. One of the ITO-electrodes was patterned. The pattern consisted of fifty $100\ \mu\text{m} \times 2\ \text{cm}$ stripes with $5\ \mu\text{m}$ spacing. The polarizer was aligned to transmit light parallel to that of the incident laser polarization. The back mirror was an Au-coated silicon substrate. Narrow-band laser oscillation at the desired wavelength is achieved by optical feedback of the retro-reflected light from one pixel of the LC-SLR, which was electrically biased, to the laser diode. The width of the pixel was chosen such that only one mode of the bare diode chip was selected. The laser is digitally tunable by electrically biasing the individual pixels, with wavelength steps $\Delta\lambda$ determined by center-to-center separation of the adjacent pixels Δx . That is,

$$\Delta\lambda = \Lambda \cos\theta_1 \Delta x/f, \quad (1)$$

where Λ is the grating period; θ_1 is the first-order diffraction angle; f is the focal length of the lens.

The contrast ratio of the homemade LC-SLR is about 5:1. Because of high gain of the semiconductor media, the LC-SLR can achieve the desired spectral filtering function. The threshold switching voltage of the LC-SLR is $4V_{pp}$ (peak-to-peak) at 10 kHz. Complete switching from off- to on-state is achieved at $10V_{pp}$. The switching time is $\sim 175\ \text{ms}$, which is determined by the characteristics of the twisted NLC cell.

Figure 3 illustrate the narrow-band ($< 0.2\ \text{nm}$, instrument limited) output of the laser as measured by an optical spectrum analyzer (Anritzu, model MS9030). The

laser wavelength can be tuned from 636 to 643 nm discretely in 0.27 nm steps by biasing sequentially the pixels. The side-mode-suppression-ratio (SMSR) of the laser was better than 20 dB throughout this range. In Fig. 4, we plot the lasing wavelength as a function of the pixel number. It is in good agreement with the theoretical prediction according to Eq. (1). The wavelength resettability of the present laser is excellent. After switching to a different pixel, the laser wavelength is reset. Realignment of the laser cavity is not necessary. The tuning range of the laser is limited by the reflectivity of the front facet of the LD. With anti-reflection coating such that $R < 1\%$ for this facet, the tuning range of the laser can easily exceed several tens of nanometers [19]. The SMSR of the laser output can be improved if we employ LC-SLR's with higher contrast ratios.

In summary, we demonstrate a novel digitally tunable laser diode. This is realized by using a folded telescopic grating-loaded external cavity with a LC-SLR at the focal plane of the folded telescope. To demonstrate, we achieved narrow-band tunable output from 636 to 643 nm in 0.27 nm steps with a low-power red LD in a commercial laser pointer. The SMSR of the laser output was better than 20 dB throughout this range. The tuning range and SMSR is limited by the reflectivity of the front facet of the LD and contrast ratio of the LC-SLR. The wavelength switching time was $\sim 175\ \text{ms}$.

Acknowledgement: This work was partially supported by the National Science Council of the R.O.O. under various grants.

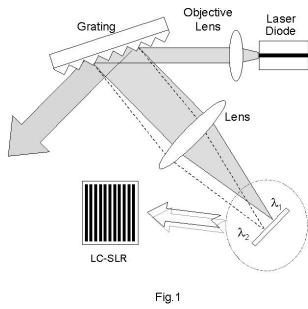


Fig.1

Fig. 1 A schematic of the digitally tunable laser. LC-SLR: Liquid Crystal Spatial Light Reflector.

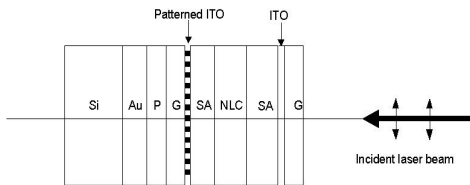


Fig.2

Fig. 2 Configuration of the LC-SLR. G: glass plate; ITO: indium-tin-oxide coating; NLC: nematic liquid crystal; SA: surface alignment layer; P: polarizer; Au: evaporated gold coating; Si: silicon substrate.

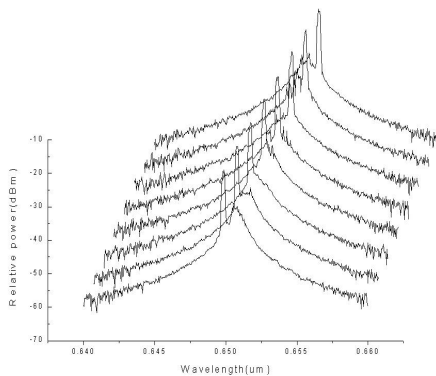


Fig.3

Fig. 3 Narrow-linewidth output spectra of the tunable laser diode.

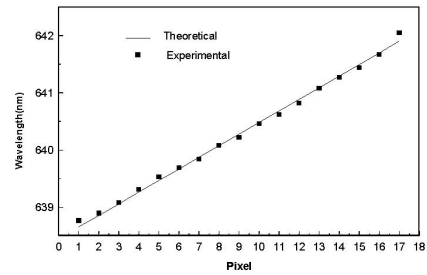


Fig.4

Fig. 4 Lasing wavelength as a Function of the pixel number. The solid line is the theoretical curve. The solid squares are experimental data.

6. 光纖光柵鎖模雷射及應用之研究

緣由與目的

近幾年來在國際上光纖光柵及光纖雷射之製作技術日趨成熟，在光纖通訊、光纖感測及超快光學上之應用也迅速地發展。藉著結合光纖光柵及光纖雷射這兩種技術，研究人員得以製作出新型之光纖雷射並發展新型之雷射應用技術。正因如此，除了各國之研究機構競相研究之外，不管是光纖光柵或光纖雷射都已有產商推出產品來賣，可見這方面的研究不只具學術價值，亦深具應用及商業價值。

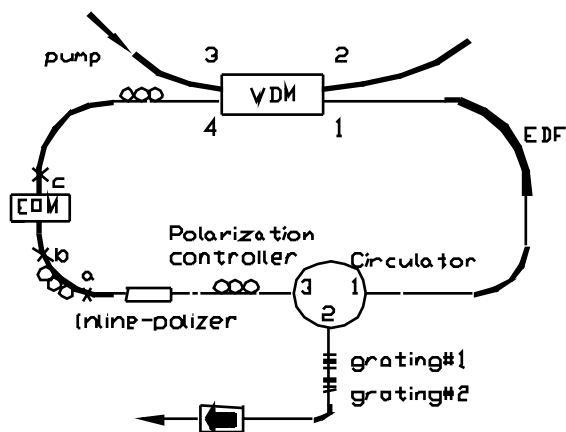
有鑑於此，我們希望結合我們已有之光纖光柵及光纖雷射製作技術來發展新型之光纖光柵鎖模雷射暨其應用，包括運用光纖光柵來作為選頻、濾波或色散補償等之各種主、被動鎖模雷射的實地研製，以及利用所研製出的雷射來發展在光纖通訊、光纖感測及超快光學及光電子學上之應用。

光纖光柵及光纖雷射之研究不但具學術價值，亦已深具應用及商業價值。結合這兩種技術所製作出的光纖光柵鎖模雷射一般就已具有可調頻、穩定、及與光纖相

容性高之優點，藉著特殊光纖光柵元件之使用，還可以針對不同的應用來發展具適當特性之雷射光源，這也是光纖光柵鎖模雷射具潛力的地方，這種在應用發展上的潛力也是本計劃之重要性所在。

結果與討論

於本計畫中我們製作了一個環狀光纖雷射腔體，利用電光相位調變器來達成主動諧波鎖模。為了解決因為超模間的彼此競爭所引起的不穩定及噪音，我們在採用由兩段具相同中心反射波長的光纖光柵所構成之反射式 Fabry-Perot 濾波器來充當雷射之輸出反射界面。雷射之整體架構如圖一中所示：

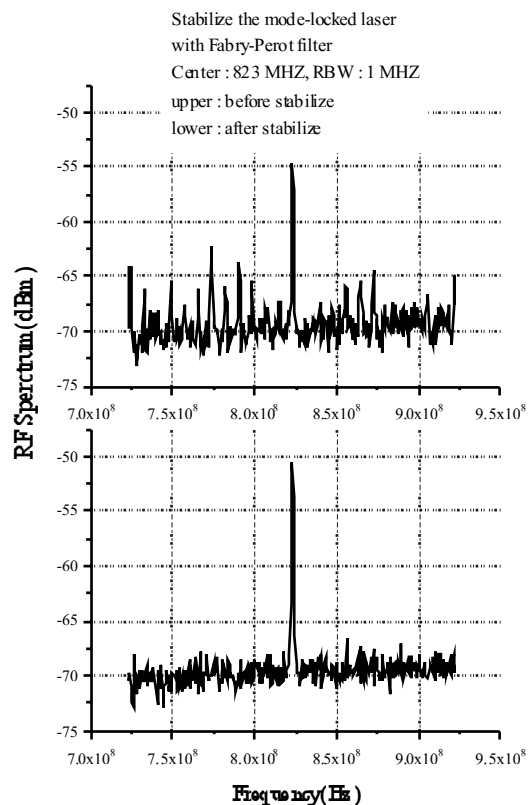


圖一·雷射架構。Grating #1 與 Grating #2 組成一個反射式的 Fabry-Perot 濾波器。EOM-電光調變器。

反射式的 Fabry-Perot 濾波器其特性與穿透式 Fabry-Perot 濾波器不同：對穿透式的濾波器而言，光纖光柵之反射率(R)越大，可以得到越佳的率波效果；但對反射式的濾波器而言，反射率越大，則濾波的效果越差。為了兼顧濾波之效果與雷射之效率，我們選擇了兩段反射率為 60% 左右的光纖光柵來做濾波。要達到穩定諧波鎖模雷射的效果，濾波器的基本共振頻率須為雷射共振腔基本共振頻率的整數倍而且應與電光調變器的調變頻率相同，這

個頻率也將正是此諧波鎖模雷射之脈衝重複率。這是因為此時雷射必須同時滿足雷射共振腔與濾波器的共振特性才能有穩定的輸出。因此我們可以藉由控制此兩段光纖光柵之間的距離，來選擇所要的脈衝重複率。

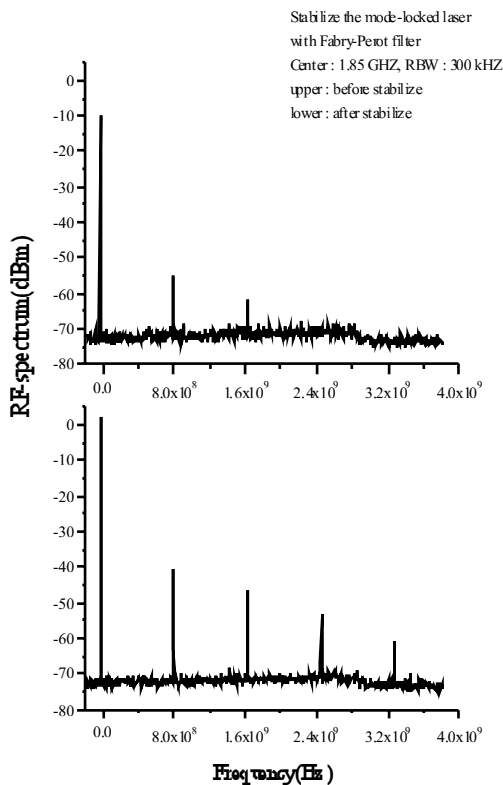
我們的實驗結果發現，於雷射腔體中置入一個反射式的光纖光柵 Fabry-Perot 濾波器可以有效地抑制旁模(sidemode)的產生(圖二)，達到穩定雷射的目的【旁模抑制比(side-mode suppression ratio)可達 40 dB 以上】。雷射的輸出 RF 頻寬(圖三)較未穩定前要寬一些，這表示脈衝寬度也變得較小些，功率輸出也比未穩定前要來的好(在 100mW 之 980nm 激發光的激發下，平均輸出功率約 3mW，power slope efficiency 由先前之 3.12% 增至 4.63%)。



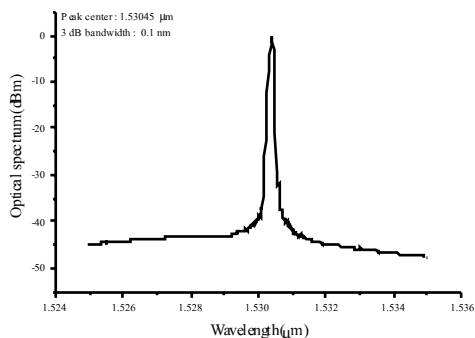
圖二·頻譜分析儀上看到旁模抑制

此雷射的典型輸出光譜與脈衝波形請見圖

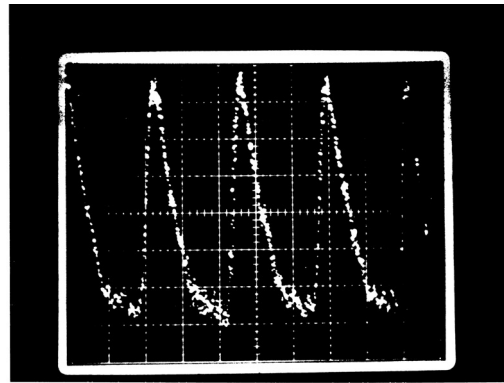
四到圖六。脈衝之寬度約為 91 ps、重複頻率為 800 MHz。我們也量測了此雷射之功率穩定度，發現平均輸出功率之混亂度在 0.5% 以內。這些成果已經很接近實用的階段，只除了脈衝重複率還要提升，脈衝寬度要再降低，以及旁模抑制比還要再增加。



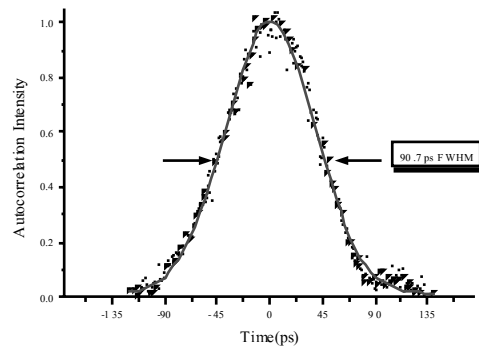
圖三·頻譜分析儀上看到的頻寬增加



圖四·雷射之輸出光譜



圖五·雷射輸出在快速示波器上之波形



圖六·雷射輸出脈衝之自相關量測結果

計畫成果自評

基本上本計畫已成功地發展出一種穩定之高重複率光纖光柵鎖模雷射，如能再作進一步之研發，此種雷射應該有潛力可以在光纖通訊及感測的應用上找到發揮的空間。所以本計畫之基本研發目標已經達成，接下來的工作則是要繼續改進雷射的架構及效果以及發展這種雷射的應用。本計畫的成果已經向中華民國的專利局申請專利，也已在 1998 年在台北舉辦的國際光電會議 (IPC'98) 中發表。【K.-H. Tu, C.-B. Huang, R.-K. Lee, and Y. Lai, "Performance of an Active Harmonic Modelocked Er-Fiber Laser Stabilized by a Reflective Fiber Grating Resonator", IPC'98, paper W-T2-B4.】，同時也將在 1999 年 CLEO 國際會議上發表。

三、參考文獻

References

1. Jia-Min Shieh, Shang-Cheng Liu and Ci-Ling Pan, *J. Opt. Soc. Am.* **B15**, 1802 (1998).
2. Hidemi Tsuchida, *Opt. Lett.* **23**, 286 (1998)
3. Jia-Min Shieh, T. C. Huang, K. F. Huang, Chi-Luen Wang, and Ci-Ling Pan, *Optics Communications*, **156**(1-3), 53 (1998).
4. S. Tsuda, W. H. Knox, S. T. Cundiff, W. Y. Jan, and J. E. Cunningham, *IEEE Sel. Topics Quantum Electron.* **2**, 454.(1996).
5. U. Keller, K. J. Weingarten, F. X. Kartner, D. Kopf, B. Braun, I. D. Jung, R. Fluck, C. Honninger, N. Matuschek, and J. A. der Au, *IEEE J. Sel. Topics Quantum Electron.* **2**, 435 (1996).
6. Jia-Min Shieh, T. C. Huang, K. F. Huang, Chi-Luen Wang, and Ci-Ling Pan, *Optics Comm.*, 156, 53 (1998) .
7. S.Tsuda et al, *IEEE Sel. Topics Quantum Electron.* **2**, 454 (1996).
8. M. J. Hayduk et al, *Optics Comm.*, 137,55 (1997)
9. U. Keller et al, *IEEE J. Sel. Topics Quantum Electron.* **2**, 435 (1996).
10. Jia-Min Shieh, T. C. Huang, K. F. Huang, Chi-Luen Wang, and Ci-Ling Pan, *Optics Communications*, 156(1-3), 53 (1998).
11. D. L. Smith and C. Mailhot, *Phys. Rev. Lett.* **58**,1264, 1987.
12. B. R. Bennet et al, *IEEE J. Quantum Electron.* **26**, 113, 1990.
13. H. Ghafour-Shiraz, Pen Wei Tan, and T. Aruga, "Picosecond Pulse Amplification in Tapered-Waveguide Laser-diode Amplifiers," *IEEE J. Sel. Topics in Quantum Electron.*, vol. 3, no. 2, pp. 210-217, 1997.
14. B. Dagens, S. Balsamo, and I. Montrosset, "Picosecond Pulse Amplification in AlGaAs flared Amplifiers," *ibid.*, pp. 233-244, 1997.
15. A. Mar, R. Helkey, J. Bowers, D. Mehuys, and D. Welch, "High Power Mode-Locked Compound Laser Using a Tapered Semiconductor Amplifier," *IEEE Photonics Technol. Lett.*, vol. 6, No. 9, pp. 1070-1072, 1994.
16. L. Goldberg, D. Mehuys, and D. Welch, "High Power Mode-Locked Compound Laser Using a Tapered Semiconductor Amplifier," *ibid.*, pp. 1070-1072, 1994.
17. Jia-Min Shieh, Hwa-Ming Twu, and Ci-Ling Pan, "Effects of intracavity dispersion on the starting dynamics of continuous-wave passively mode-locked Ti:sapphire/DDI lasers," *Opt. Lett.*, Vol.21, No.14 1058-1060 (1996)
18. P. Zorabedian, "Tunable External-Cavity Semiconductor Lasers," in F. J. Duarte, ed., *Tunable Lasers Handbook*, 1995, Academic Press, San Diego, Chapter 8.
19. Ci-Ling Pan and Chi-Luen Wang, *Opt. Quantum Electron.* Vol. 28, pp. 1239 – 1257, 1996. And references therein.
20. Harvey et al, *Optics Letters* vol.18, No.2, 15 Jan. 1993, pp. 107-107.
21. Wey et al., *IEEE J. of Lightwave Tech.* Vol.15, No.7, July 1997, pp.1171-1180.
22. Shan et al, *Electronics Letters* Vol.32, No.11, May 23 1996, pp.1015-1016.
23. Nakazawa et al, *Jpn. J. Appl. Phys.* Vol.35, No.6A, June 1996, pp. L691-L694.
24. Nakazawa et al., *Electronics Letters* Vol.32, No.5, FEB 29 1996, pp.461-463.